XA27 Depends on an Amino-Terminal Signal-Anchor-Like Sequence to Localize to the Apoplast for Resistance to *Xanthomonas oryzae* pv *oryzae*[1][W]

Lifang Wu, Mei Ling Goh, Chellamma Sreekala[2], and Zhongchao Yin*

Temasek Life Sciences Laboratory, National University of Singapore, Singapore 117604, Republic of Singapore

The rice (*Oryza sativa*) gene *Xa27* confers resistance to *Xanthomonas oryzae* pv *oryzae*, the causal agent of bacterial blight disease in rice. Sequence analysis of the deduced XA27 protein provides little or no clue to its mode of action, except that a signal-anchor-like sequence is predicted at the amino (N)-terminal region of XA27. As part of an effort to characterize the biochemical function of XA27, we decided to determine its subcellular localization. Initial studies showed that a functional XA27-green fluorescent protein fusion protein accumulated in vascular elements, the host sites where the bacterial blight pathogens multiply. The localization of XA27-green fluorescent protein to the apoplast was verified by detection of the protein on cell walls of leaf sheath and root cells after plasmolysis. Similarly, XA27-FLAG localizes to xylem vessels and cell walls of xylem parenchyma cells, revealed by immunogold electron microscopy. XA27-FLAG could be secreted from electron-dense vesicles in cytoplasm to the apoplast via exocytosis. The signal-anchor-like sequence has an N-terminal positively charged region including a triple arginine motif followed by a hydrophobic region. Deletion of the hydrophobic region or substitution of the triple arginine motif with glycine or lysine residues abolished the localization of the mutated proteins to the cell wall and impaired the plant's resistance to *X. oryzae* pv *oryzae*. These results indicate that XA27 depends on the N-terminal signal-anchor-like sequence to localize to the apoplast and that this localization is important for resistance to *X. oryzae* pv *oryzae*.

Plant disease resistance (*R*) genes confer race-specific resistance to pathogens that have cognate avirulence (*Avr*) genes (Flor, 1971). The R protein presumably functions as part of a receptor complex that recognizes the Avr protein and subsequently initiates defense responses (Hammond-Kosack and Jones, 1997; Martin et al., 2003). The majority of R proteins fall into five classes based primarily upon the combination of a limited number of structural motifs that they contain, while a few other R proteins have novel structures (Dangl and Jones, 2001; Martin et al., 2003). One of the interesting aspects of R protein function is their subcellular localization. Several examples of direct physical interactions between R and Avr proteins have been demonstrated (Scofield et al., 1996; Tang et al., 1996; Jia et al., 2000; Leister and Katagiri, 2000; Kim et al., 2002). Viral effectors are present inside the plant cell, and the predicted structures of all known R proteins against viruses indicate that they are also intracellular (Burch-Smith et al., 2007). The tomato (*Solanum lycopersicum*) Cf proteins, which recognize extracellular *Cladosporium fulvum* Avr proteins (Lauge and De Wit, 1998), are localized to the plasma membrane (Rivas and Thomas, 2005). Fungal pathogen-directed R proteins can also be intracellular, as fungal Avr proteins are delivered to and function inside plant cells (Jia et al., 2000). Similarly, all bacteria-directed R proteins are predicted to be intracellular, with the exception of XA21 (Song et al., 1995), because most of the bacterial *Avr* effector proteins are secreted into the host cells through the bacterial type III secretion system (He et al., 2004).

However, many R proteins do not carry recognizable subcellular targeting signatures, and their actual subcellular localization needs to be determined experimentally. For instance, Arabidopsis (*Arabidopsis thaliana*) RPM1 and RPS2 are associated with cellular membranes, although they do not possess any canonical membrane-targeting domains (Boyes et al., 1998; Axtell and Staskawicz, 2003). This subcellular localization is consistent with the membrane localization of their corresponding Avr elicitors, AvrRpm1 and AvrRpt2, respectively (Nimchuk et al., 2000; Axtell and Staskawicz, 2003). Apart from the plasma membrane, Arabidopsis RRS1-R and its cognate Avr protein PopP2 colocalize to the nucleus, and the nuclear localization of RRS1-R is dependent on the presence of PopP2 (Deslandes et al., 2003). Recently, both tobacco (*Nicotiana tabacum*) N and barley (*Hordeum vulgare*) MLA10 were found to localize to the cytoplasm as well as the nucleus, and the nuclear retention of either R

[1] This work was supported by intramural research funds from the Temasek Life Sciences Laboratory (to Z.Y.) and by a grant from the Agri-Food and Veterinary Authority of Singapore (to Z.Y.).

[2] Present address: Molecular Genetics, Agriculture and Agri-Food Canada, 107 Science Place, Saskatoon, Saskatchewan, Canada S7N 0X2.

* Corresponding author; e-mail yinzc@tll.org.sg.

The author responsible for distribution of materials integral to the findings presented in this article in accordance with the policy described in the Instructions for Authors (www.plantphysiol.org) is: Zhongchao Yin (yinzc@tll.org.sg).

[W] The online version of this article contains Web-only data.
www.plantphysiol.org/cgi/doi/10.1104/pp.108.123356

protein is indispensable for downstream signaling and defense (Burch-Smith et al., 2007; Shen et al., 2007). In these three cases, translocation of the R proteins during signaling might take place upon activation of the R proteins by the cognate Avr proteins (Deslandes et al., 2003; Burch-Smith et al., 2007; Shen et al., 2007). Rice (*Oryza sativa*) XA21 is a transmembrane receptor kinase that presumably recognizes an elicitor localized to the apoplast of rice cells, with its extracellular Leu-rich repeat domain (Song et al., 1995). The AvrXa21 molecule(s) corresponding to XA21 has yet to be identified, although it appears that it might be a sulfated protein secreted to the apoplast through a type I secretion system and involved in quorum sensing (Lee et al., 2006).

Bacterial blight, caused by *Xanthomonas oryzae* pv *oryzae*, is one of the most destructive bacterial diseases of rice (Mew, 1987). We previously reported the isolation of the resistance gene, *Xa27*, from rice (Gu et al., 2005). *Xa27*-dependent resistance is associated with the specific induction of the *Xa27* gene by incompatible pathogens harboring *avrXa27*. Unlike other cloned *R* genes, the resistance specificity of *Xa27* to various *X. oryzae* pv *oryzae* strains is determined by its promoter rather than by its gene product. Indeed, ectopic expression of the *Xa27* coding region under the control of the rice *PR1* promoter resulted in nonspecific resistance to both incompatible and compatible strains. The *Xa27* gene encodes a predicted protein of 113 amino acid residues that lacks known functional domains that might provide a clue to its function. Interestingly, a signal-anchor-like sequence was predicted at the N-terminal region of XA27 by SignalP-HMM (http://www.cbs.dtu.dk/services/SignalP/; $P = 0.790$; Fig. 1). The signal-anchor-like sequence contains 37 positively charged amino acids, including a triple Arg motif from residues 27 to 29 (n-region), followed by a 20-amino acid hydrophobic region (h-region; Emanuelsson et al., 2007). Signal anchor sequences initiate translocation in the same manner as signal peptides, but they are not cleaved by signal peptidase after protein translocation, resulting in membrane association of the protein (von Heijne, 1988). As part of our effort to characterize the biochemical function of XA27, we carried out studies on its subcellular localization. We examined the function of its signal-anchor-like sequence and the relationship between XA27 localization and resistance to *X. oryzae* pv *oryzae*.

RESULTS

Functional XA27-GFP Localizes to the Apoplast

To investigate XA27 localization, we generated transgenic plants in a Nipponbare background that carried an *XA27-GFP* fusion gene under the control of either the native *Xa27* promoter (P_{Xa27}:*XA27-GFP*:T_{Xa27}) or the maize (*Zea mays*) ubiquitin gene promoter (P_{Ubi}: *XA27-GFP*:T_{Nos}; Table I). Seven resistant transgenic P_{Xa27}:*XA27-GFP*:T_{Xa27} lines were generated, and line 22 (L22) was selected for further analysis. L22 carried a single copy of the P_{Xa27}:*XA27-GFP*:T_{Xa27} gene and retained race-specific resistance to PXO99^{A} (Fig. 2A; Table II). The P_{Xa27}:*XA27-GFP*:T_{Xa27} gene in L22 expressed at a low level constitutively, which might have resulted from leaky activity of the *Xa27* promoter (Fig. 2B). The P_{Xa27}:*XA27-GFP*:T_{Xa27} gene in L22 was induced after inoculation with PXO99^{A} but not with compatible *X. oryzae* pv *oryzae* strain PXO99^{A}ME1, in which *avrXa27* is disrupted (Gu et al., 2005; Fig. 2B). Thirty-three independent transgenic P_{Ubi}:*XA27-GFP*:T_{Nos} lines were produced, and their disease phenotype after inoculation with PXO99^{A} varied from complete susceptibility to full resistance in the T_0 generation (data not shown). Line 9 (L9) of P_{Ubi}:*XA27-GFP*:T_{Nos} was selected for further study. The P_{Ubi}:*XA27-GFP*:T_{Nos} gene in L9 was expressed constitutively at a high level (Fig. 2C). L9 conferred resistance to both PXO99^{A} and PXO99^{A}ME1 in T1 and in subsequent generations (Fig. 2, A and C; Table II). Compared with L22 and line 8 (L8) of P_{Ubi}:*GFP*:T_{Nos} (Fig. 2A; Tables I and II), L9 displayed phenotypic changes, including inhibition of tillering, delay in flowering, stiff leaves, and early leaf senescence, which might have resulted from overexpression of the P_{Ubi}:*XA27-GFP*:T_{Nos} gene (data not shown).

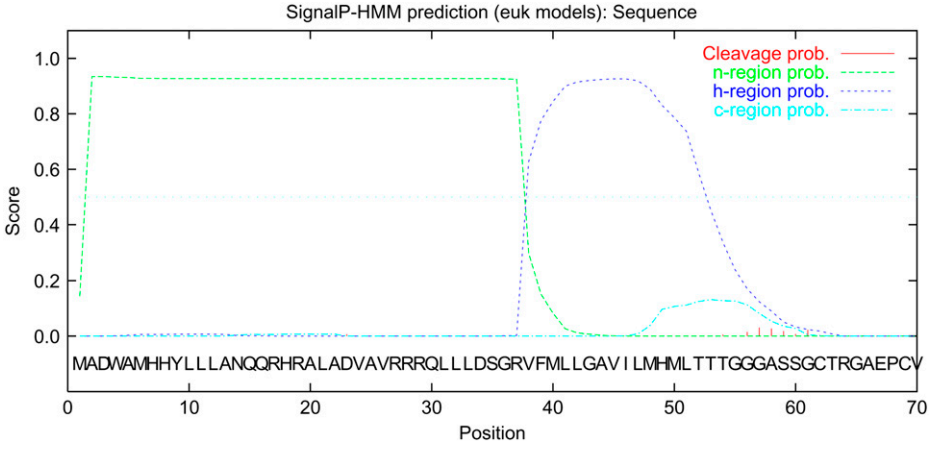

Figure 1. Output of SignalP-HMM prediction of XA27 from the SignalP 3.0 server. A signal-anchor-like sequence was predicted at the N-terminal region of XA27, which contains an N-terminal positively charged region (n-region; residues 1–37) followed by a hydrophobic region (h-region; residues 38–57; Emanuelsson et al., 2007). The full-length amino acid sequence of XA27 was submitted to the SignalP 3.0 server (http://www.cbs.dtu.dk/services/SignalP/) for prediction of the signal peptide or signal anchor of eukaryotes. Methods of both neural networks and hidden Markov models were used for prediction. Standard output format was selected.

Table I. *Constructs used in this study*

Construct	Gene of Interest in the Construct[a]	Reference
NA5.2	Wild-type *Xa27* (IRBB27 allele)	Gu et al. (2005)
pSSZ41	P_{Ubi}:*GFP*:T_{Nos}	Kolesnik et al. (2004)
pCUXA27GFP	P_{Ubi}:*XA27-GFP*:T_{Nos}	This study
pC27XA27GFP	P_{Xa27}:*XA27-GFP*:T_{Xa27}	This study
pC27XA27FLAG	P_{Xa27}:*XA27-FLAG*:T_{Xa27}	This study
pCUN57GFP	P_{Ubi}:*N57-GFP*:T_{Nos}	This study
pCUN37GFP	P_{Ubi}:*N37-GFP*:T_{Nos}	This study
pCUN57GGFP	P_{Ubi}:*N57G-GFP*:T_{Nos}	This study
pCUN57KGFP	P_{Ubi}:*N57K-GFP*:T_{Nos}	This study
pCUXA27GGFP	P_{Ubi}:*XA27G-GFP*:T_{Nos}	This study
pC27XA27GGFP	P_{Xa27}:*XA27G-GFP*:T_{Xa27}	This study
pC27XA27G	P_{Xa27}:*XA27G*:T_{Xa27}	This study

[a] P_{Ubi}, Maize ubiquitin gene promoter; *GFP*, coding region of the GFP gene (accession no. AAB92477); T_{Nos}, terminator of the nopaline synthase gene (*Nos*); P_{Xa27}, *Xa27* promoter; T_{Xa27}, *Xa27* terminator; *XA27-GFP*, fusion gene encoding XA27-GFP; *XA27-FLAG*, fusion gene encoding XA27-FLAG; *N57-GFP*, fusion gene encoding N57-GFP; *N37-GFP*, fusion gene encoding N37-GFP; *N57G-GFP*, fusion gene encoding N57G-GFP; *N57K-GFP*, fusion gene encoding N57K-GFP; *XA27G-GFP*, fusion gene encoding XA27G-GFP; *XA27G*, *Xa27* mutant encoding XA27G. For generation of fusion or mutated genes, see "Materials and Methods."

Leaf cross sections from the immediate vicinity of the infected sites in L8 of P_{Ubi}:*GFP*:T_{Nos}, L9 of P_{Ubi}:*XA27-GFP*:T_{Nos}, and L22 of P_{Xa27}:*XA27-GFP*:T_{Xa27} were subjected to confocal microscopy. The GFP fluorescence in L8 was strong, especially in mesophyll parenchyma cells (Fig. 3A). Although the fluorescence intensity in L9 was weaker than that in L8, the XA27-GFP protein was evenly distributed among vascular bundles and mesophyll tissues (Fig. 3B). The expression of GFP in L8 or XA27-GFP in L9 did not change after bacterial inoculation with PXO99^A (data not shown). A low level of XA27-GFP was detected in uninoculated L22 plants, due to leaky expression of the P_{Xa27}:*XA27-GFP*:T_{Xa27} gene (Fig. 3C). XA27-GFP was strongly induced in vascular bundles of L22 plants at 3 d after inoculation (DAI) with PXO99^A. It was mainly accumulated in the vascular elements, including xylem vessels, protoxylem, and phloem (Fig. 3D). However, the expression of P_{Xa27}:*XA27-GFP*:T_{Xa27} in mesophyll parenchyma cells of L22 did not change significantly after bacterial inoculation (Fig. 3, C and D).

How does XA27-GFP come to be localized in xylem vessels and protoxylem, which consist of apoplast structures? One possibility is that it might be secreted from the neighboring xylem parenchyma cells. To test this possibility, we studied the localization of XA27-GFP in leaf sheath and root cells of L9 and L22. To make it easy to identify the cell wall, we induced plasmolysis in the leaf sheath or root tissues by treatment with a high-osmolarity solution. The control GFP protein in L8 was found in both the cytosol and the nucleus (Fig. 4, A and C; Supplemental Fig. S1A). After plasmolysis, no GFP protein was detected on the cell walls of leaf sheath or root cells of L8 (Fig. 4, B and D). In contrast, fluorescent spots appeared along the borders of leaf sheath cells of L9, which could be XA27-GFP-containing vesicles (see below; Fig. 4E). After plasmolysis, XA27-GFP was detected on the cell walls of both leaf sheath and root cells (Fig. 4, F and H). Compared with leaf sheath cells, XA27-GFP was more evenly distributed on root cell walls (Fig. 4G). In addition, XA27-GFP proteins were detected in the perinuclear region, producing a fluorescent nuclear halo (Fig. 4, E and G). 4′,6-Diamidino-2-phenylindole staining also indicated that XA27-GFP did not localize to the nucleus (Supplemental Fig. S1B). This perinuclear protein might be associated with the endoplasmic reticulum. Although a smaller amount of XA27-GFP was detected in L22, the localization patterns of XA27-GFP in the leaf sheath and the root cells of L22 were similar to that in L9 (Supplemental Fig. S2).

XA27-FLAG Translocates to the Apoplast via Electron-Dense Vesicles

To further determine the subcellular localization of XA27, we fused XA27 with the FLAG epitope tag and performed immunogold electron microscopy to visualize XA27-FLAG in transgenic P_{Xa27}:*XA27-FLAG*:T_{Xa27} plants (XA27-GFP could not be recognized by commercial anti-GFP antibodies). Forty-three independent transgenic P_{Xa27}:*XA27-FLAG*:T_{Xa27} lines were generated. Line 18 (L18F) was selected for further analysis because it carried a single copy of the P_{Xa27}:*XA27-FLAG*:T_{Xa27} gene. This line conferred complete resistance to PXO99^A and displayed moderate susceptibility to PXO99^{A}ME1 (Fig. 2A; Table II). The P_{Xa27}:*XA27-FLAG*:T_{Xa27} gene in L18F was expressed constitutively at a low level but was inducible upon inoculation with PXO99^A (Fig. 2D). The XA27-FLAG protein in L18F was detected as a band with a molecular size of about 13 kD

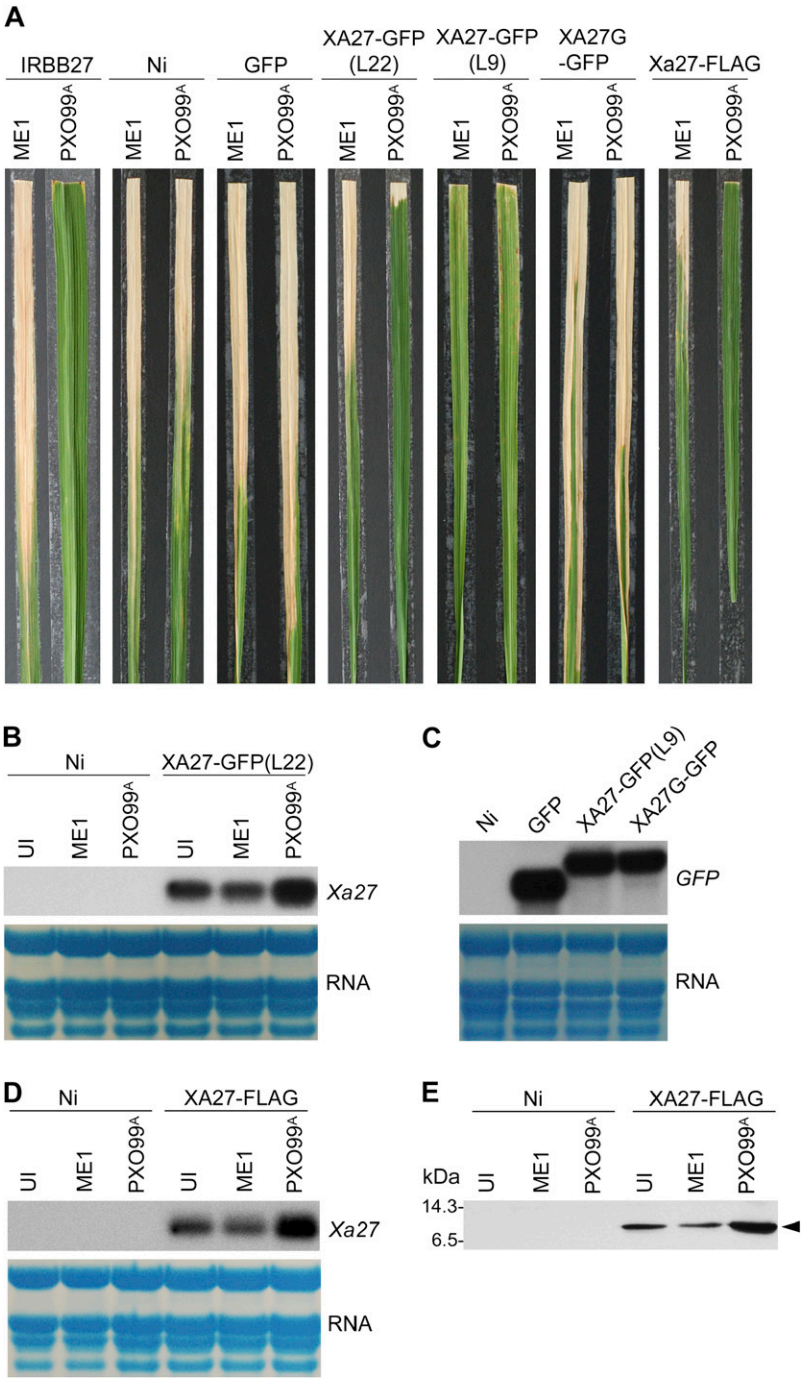

Figure 2. Generation of XA27-tagged lines. A, Disease phenotypes of XA27-tagged lines, control lines, and wild-type plants at 14 DAI with *X. oryzae* pv *oryzae* strains. Plants were inoculated with *X. oryzae* pv *oryzae* PXO99^{A} harboring wild-type *avrXa27* or *avrXa27* mutant PXO99^{A}ME1 (ME1), and photographs were taken at 14 DAI. IRBB27, wild-type *Xa27* plants; Ni, Nipponbare; GFP, L8 of P_{Ubi}:*GFP*:T_{Nos}; XA27-GFP(L22), L22 of P_{Xa27}:*XA27-GFP*:T_{Xa27}; XA27-GFP(L9), L9 of P_{Ubi}:*XA27-GFP*:T_{Nos}; XA27G-GFP, L18G of P_{Ubi}:*XA27G-GFP*:T_{Nos}; XA27-FLAG, L18F of P_{Xa27}:*XA27-FLAG*:T_{Xa27}. B, Expression of P_{Xa27}:*XA27-GFP*:T_{Xa27} in uninoculated (UI) L22 plants or L22 plants at 3 DAI with *X. oryzae* pv *oryzae* strains PXO99^{A}ME1(ME1) and PXO99^{A}. Nipponbare (Ni) was used as a control. C, Ubiquitin promoter-driven *GFP*, *XA27-GFP*, and *XA27G-GFP* gene expression in transgenic lines. GFP, L8 of P_{Ubi}:*GFP*:T_{Nos}; XA27-GFP(L9), L9 of P_{Ubi}:*XA27-GFP*:T_{Nos}; XA27G-GFP, L18G of P_{Ubi}:*XA27G-GFP*:T_{Nos}. Nipponbare (Ni) was used as a control. D, Expression of P_{Xa27}:*XA27-FLAG*:T_{Xa27} in uninoculated (UI) L18F plants or L18F plants at 3 DAI with PXO99^{A}ME1(ME1) or PXO99^{A}. Nipponbare (Ni) was used as a control. E, Expression of XA27-FLAG in uninoculated (UI) L18F plants or L18F plants at 3 DAI with PXO99^{A}ME1(ME1) or PXO99^{A}. Nipponbare (Ni) was used as a control. XA27-FLAG was detected with anti-FLAG monoclonal antibodies. The molecular mass values of standard protein markers (Amersham Biosciences; RPN755) are shown in kilodaltons. The position of XA27-FLAG is indicated (arrowhead).

in immunoblot analysis with anti-FLAG monoclonal antibody (Fig. 2E).

Leaf cross sections of L18F plants were subjected to immunogold electron microscopy. As depicted by the gold particles, XA27-FLAG was detected in the cytoplasm and the apoplast of the xylem parenchyma cells (Fig. 5, E–L). In uninoculated L18F plants, XA27-FLAG localized mainly to electron-dense vesicles in the cytoplasm and to the cell walls of xylem parenchyma cells (Fig. 5, E and F). After inoculation with PXO99^{A}, XA27-FLAG protein was induced to higher levels in the xylem parenchyma cells of L18F plants. Electron-dense vesicles containing XA27-FLAG were abundant at the pits between xylem parenchyma cells (Fig. 5, G–I), between xylem vessels and parenchyma cells (Fig. 5, J–K), and between xylem parenchyma cells and mesophyll parenchyma cells (data not shown). The XA27-FLAG protein was also found in the xylem vessels of inoculated L18F plants, where it localized to lumina of the xylem vessels rather than being associated with bacteria or vessel walls (Fig. 5L). XA27-FLAG appears to be secreted from electron-

Table II. *Disease evaluation of selected transgenic lines and wild-type plants to X. oryzae pv oryzae strains PXO99^A and PXO99^{A}ME1*

Line	Gene[a]	Lesion Length (*cm*) and Disease Score[b]	
		PXO99^A	PXO99^{A}ME1
IRBB27	*Xa27*	0.3 ± 0.2 (R)	25.4 ± 4.7 (S)
Nipponbare	*xa27*(Ni)	14.5 ± 4.0 (S)	15.0 ± 2.8 (S)
L8	P_{Ubi}:*GFP*:T_{Nos}	15.6 ± 2.7 (S)	15.6 ± 2.6 (S)
L22	P_{Xa27}:*XA27-GFP*:T_{Xa27}	0.7 ± 0.9 (R)	13.3 ± 3.0 (S)
L18F	P_{Xa27}:*XA27-FLAG*:T_{Xa27}	0.2 ± 0.1 (R)	6.3 ± 1.7 (MS)
L9	P_{Ubi}:*XA27-GFP*:T_{Nos}	0.9 ± 1.1 (R)	3.0 ± 0.9 (R)
L12	P_{Ubi}:*N57-GFP*:T_{Nos}	16.0 ± 1.7 (S)	16.6 ± 4.4 (S)
L2	P_{Ubi}:*N37-GFP*:T_{Nos}	14.3 ± 0.4 (S)	15.9 ± 3.1 (S)
L5	P_{Ubi}:*N57G-GFP*:T_{Nos}	13.3 ± 2.8 (S)	14.7 ± 1.6 (S)
L3	P_{Ubi}:*N57K-GFP*:T_{Nos}	15.0 ± 1.7 (S)	15.2 ± 0.8 (S)
L18G	P_{Ubi}:*XA27G-GFP*:T_{Nos}	10.4 ± 1.8 (S)	13.9 ± 4.2 (S)
L46	P_{Xa27}:*XA27G-GFP*:T_{Xa27}	11.6 ± 3.2 (S)	14.9 ± 4.1 (S)

[a]For genes, refer to the genes of interest in the constructs in Table I. *xa27*(Ni), Susceptible allele of the *Xa27* gene in Nipponbare. [b]The lesion length is the average of 16 infected leaves. The SD of the mean is indicated. MS, Moderately susceptible; R, resistant; S, susceptible.

dense vesicles in the cytoplasm to the apoplast, perhaps via exocytosis (Fig. 5H). No XA27-FLAG protein was found to localize to the nucleus or other organelles of xylem parenchyma cells in either uninoculated or inoculated L18F plants (data not shown). In control experiments, in which preimmune serum was used to replace anti-FLAG antibody, we did not observe concentrated labeling of vesicular structures in specimens of L18F (Fig. 5, A and B). Similar results were obtained with samples of Nipponbare lacking the transgene when anti-FLAG antibody was used (Fig. 5, C and D).

The N-Terminal Signal-Anchor-Like Sequence Is Required for XA27 Localization

To determine whether the signal-anchor-like sequence is sufficient to explain the observed localization of XA27 to the apoplast and cell wall, we fused this sequence to GFP (N57-GFP) and generated 56 transgenic plants with the P_{Ubi}:*N57-GFP*:T_{Nos} gene (Table I). Line 12 (L12) of P_{Ubi}:*N57-GFP*:T_{Nos} was selected to study N57-GFP localization (Table II). The expression of the P_{Ubi}:*N57-GFP*:T_{Nos} gene in L12 was comparable to that of the P_{Ubi}:*GFP*:T_{Nos} gene in L8 (Supplemental Fig. S3). Like XA27-GFP, N57-GFP localized to the cell walls of leaf sheath and root cells (Fig. 6, A to D).

To determine whether the h-region of the signal-anchor-like sequence is required for this localization, we deleted the h-region from the signal-anchor-like sequence and fused the remaining 37-amino acid n-region with GFP (N37-GFP). We generated 66 transgenic plants with the P_{Ubi}:*N37-GFP*:T_{Nos} gene (Table I). Line 2 (L2) of P_{Ubi}:*N37-GFP*:T_{Nos} was selected to study N37-GFP localization (Table II; Supplemental Fig. S3). After plasmolysis, no N37-GFP was detected on the cell walls of leaf sheath or of root cells (Fig. 6, E and F).

The triple Arg motif in the signal-anchor-like sequence of XA27 is conserved between XA27 and its paralogs in rice (Gu et al., 2005). To determine the function of this triple Arg motif in protein localization, we replaced it with Gly or Lys residues and generated transgenic plants with the mutated fusion genes P_{Xa27}:*XA27G-GFP*:T_{Xa27}, P_{Ubi}:*XA27G-GFP*:T_{Nos}, P_{Ubi}:*N57G-GFP*:T_{Nos}, and P_{Ubi}:*N57K-GFP*:T_{Nos} (Table I). Line 46 (L46) of P_{Xa27}:*XA27G-GFP*:T_{Xa27}, line 18 (L18G) of P_{Ubi}:*XA27G-GFP*:T_{Nos}, line 5 (L5) of P_{Ubi}:*N57G-GFP*:T_{Nos}, and line 3 (L3) of P_{Ubi}:*N57K-GFP*:T_{Nos} were selected to study the localization of these fusion proteins (Table II). Like the P_{Xa27}:*XA27-GFP*:T_{Xa27} gene in L22, the P_{Xa27}:*XA27G-GFP*:T_{Xa27} gene in L46 showed weak expression in uninoculated plants but was induced at xylem parenchyma cells after inoculation of L46 plants with PXO99^A. However, the induced XA27G-GFP protein was trapped in xylem parenchyma cells and was not secreted into the apoplast or xylem vessel (Fig. 3, E and F). In addition, XA27G-GFP localized to the nucleus, detected by 4′,6-diamidino-2-phenylindole staining (Supplemental Fig. S1C). Although the expression of the P_{Ubi}:*XA27G-GFP*:T_{Nos} gene in L18G, the P_{Ubi}:*N57G-GFP*:T_{Nos} gene in L5, and the P_{Ubi}:*N57K-GFP*:T_{Nos} gene in L3 was comparable to that of the P_{Ubi}:*XA27-GFP*:T_{Nos} gene in L9 and the P_{Ubi}:*N57-GFP*:T_{Nos} gene in L12 (Fig. 2C; Supplemental Fig. S3), XA27G-GFP, N57G-GFP, and N57K-GFP failed to localize to the cell walls of either leaf sheath or root cells (Fig. 7; Supplemental Fig. S4).

Localization of XA27 to the Apoplast Is Required for Disease Resistance

The failure of localization of XA27G-GFP to the apoplast in L18G of P_{Ubi}:*XA27G-GFP*:T_{Nos} and in L46 of P_{Xa27}:*XA27G-GFP*:T_{Xa27} allowed us to ask whether the proper localization of the fusion protein is required for its function in conferring disease resistance. Plants expressing the XA27G-GFP proteins were not resistant to bacterial blight pathogens (Fig. 2A; Table II). These

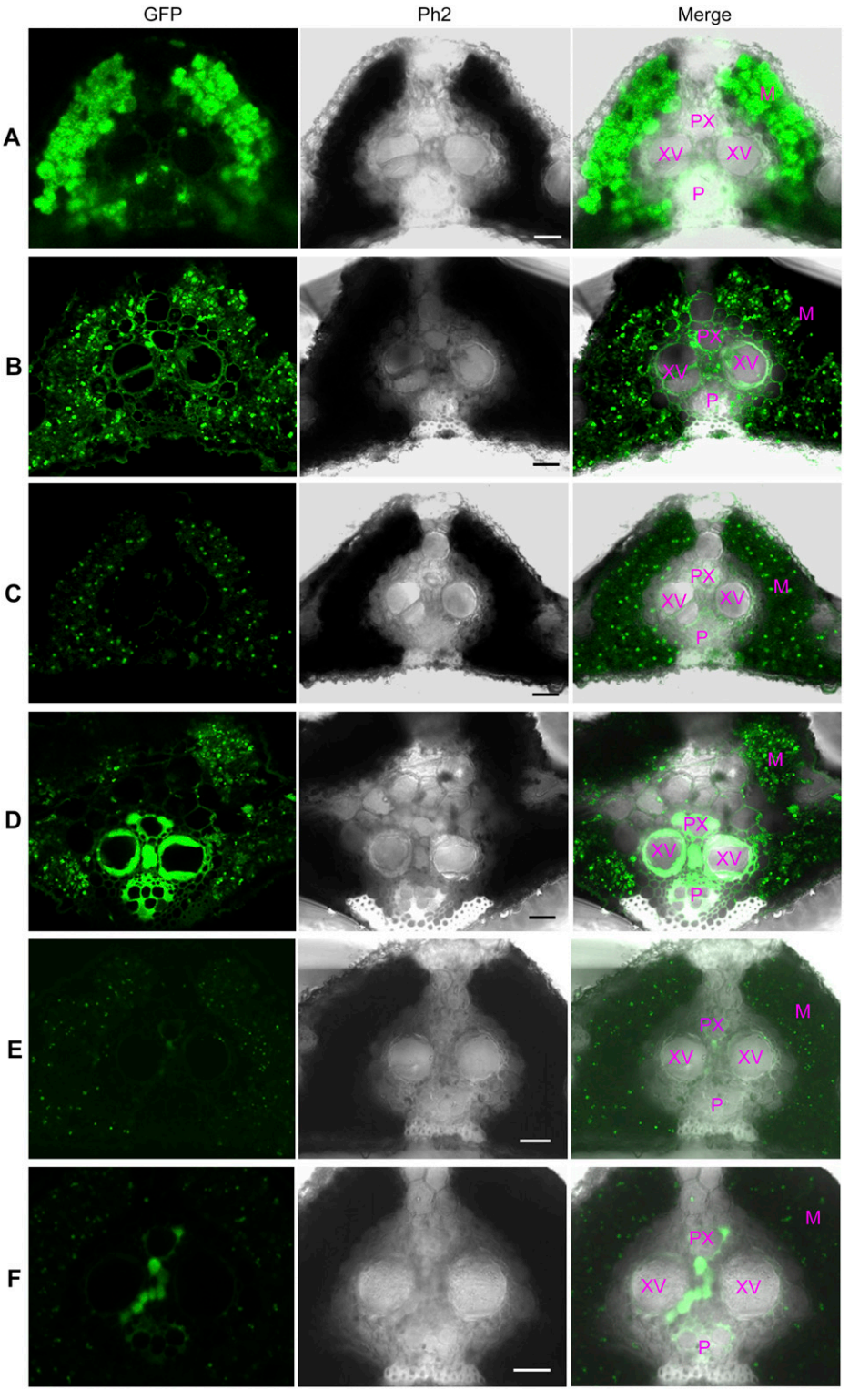

Figure 3. Expression of GFP, XA27-GFP, and XA27G-GFP in leaf cross sections of transgenic plants. A, L8 of P_{Ubi}:*GFP*:T_{Nos} at 3 DAI with *X. oryzae* pv *oryzae* PXO99^{A}. B, L9 of P_{Ubi}:*XA27-GFP*:T_{Nos} at 3 DAI with PXO99^{A}. C, L22 of P_{Xa27}:*XA27-GFP*:T_{Xa27}. D, L22 at 3 DAI with PXO99^{A}. E, L46 of P_{Xa27}:*XA27G-GFP*:T_{Xa27}. F, L46 at 3 DAI with PXO99^{A}. M, Mesophyll parenchyma cells; P, phloem; Ph2, Phase Contrast 2; PX, protoxylem; XV, xylem vessel. Bars = 20 μm.

results suggest that the localization of XA27 to the apoplast is required for XA27-mediated disease resistance to *X. oryzae* pv *oryzae*. To further test this, we replaced the triple Arg motif in XA27 with Gly residues and generated transgenic plants with the P_{Xa27}:*XA27G*:T_{Xa27} gene (Table I). Sixty-one independent transgenic lines were obtained, and they all carried the P_{Xa27}:*XA27G*:T_{Xa27} gene (data not shown). Although the expression of P_{Xa27}:*XA27G*:T_{Xa27} in these transgenic plants was comparable to that of the wild-

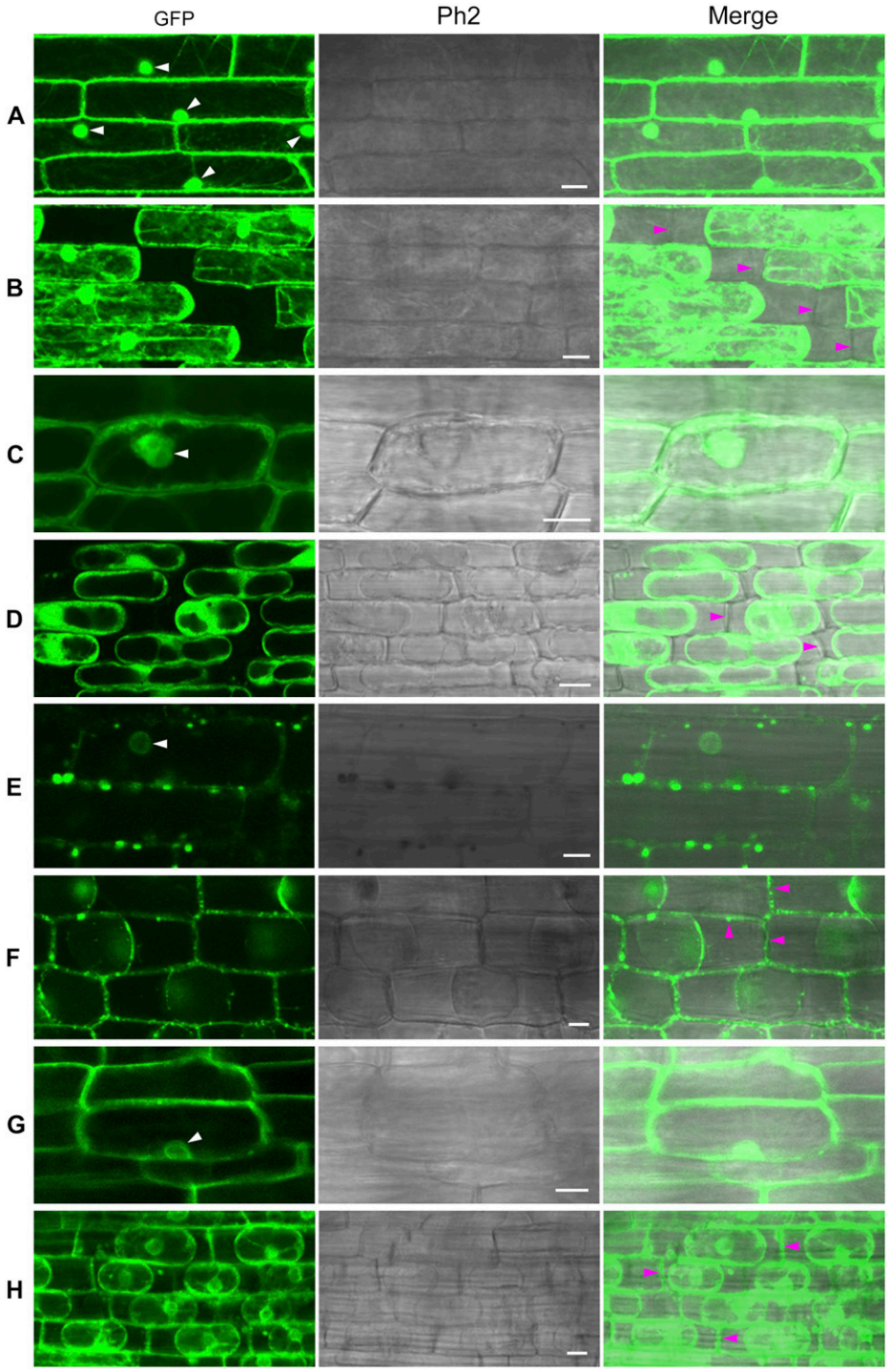

Figure 4. Localization of GFP and XA27-GFP in leaf sheath and root cells of transgenic plants. A, Leaf sheath cells of L8 of P_{Ubi}:*GFP*:T_{Nos}. B, Leaf sheath cells of L8 after plasmolysis. C, Root cells of L8. D, Root cells of L8 after plasmolysis. E, Leaf sheath cells of L9 of P_{Ubi}:*XA27-GFP*:T_{Nos}. F, Leaf sheath cells of L9 after plasmolysis. G, Root cells of L9. H, Root cells of L9 after plasmolysis. The nuclei are indicated with white arrowheads. Cell walls are indicated with magenta arrowheads. Ph2, Phase Contrast 2. Bars = 10 μm.

type *Xa27* transgene in transgenic line TN8 after inoculation with PXO99^{A} (Fig. 8B), none of the XA27G transgenic plants conferred resistance to the incompatible strain (Fig. 8A).

DISCUSSION

Xa27 is specifically induced by AvrXa27 from incompatible pathogens (Gu et al., 2005). In vivo in IRBB27, the expression of *Xa27* is normally tightly controlled and is not induced by any other biotic and abiotic stresses (Gu et al., 2005). Nonetheless, we found that constructs containing the *Xa27* promoter showed constitutive low-level expression in transgenic plants. This was true whether the transgenic plants contained genomic clones of *Xa27* under the control of its native promoter (L. Wu and Z. Yin, unpublished data) or fusion genes under the control of the

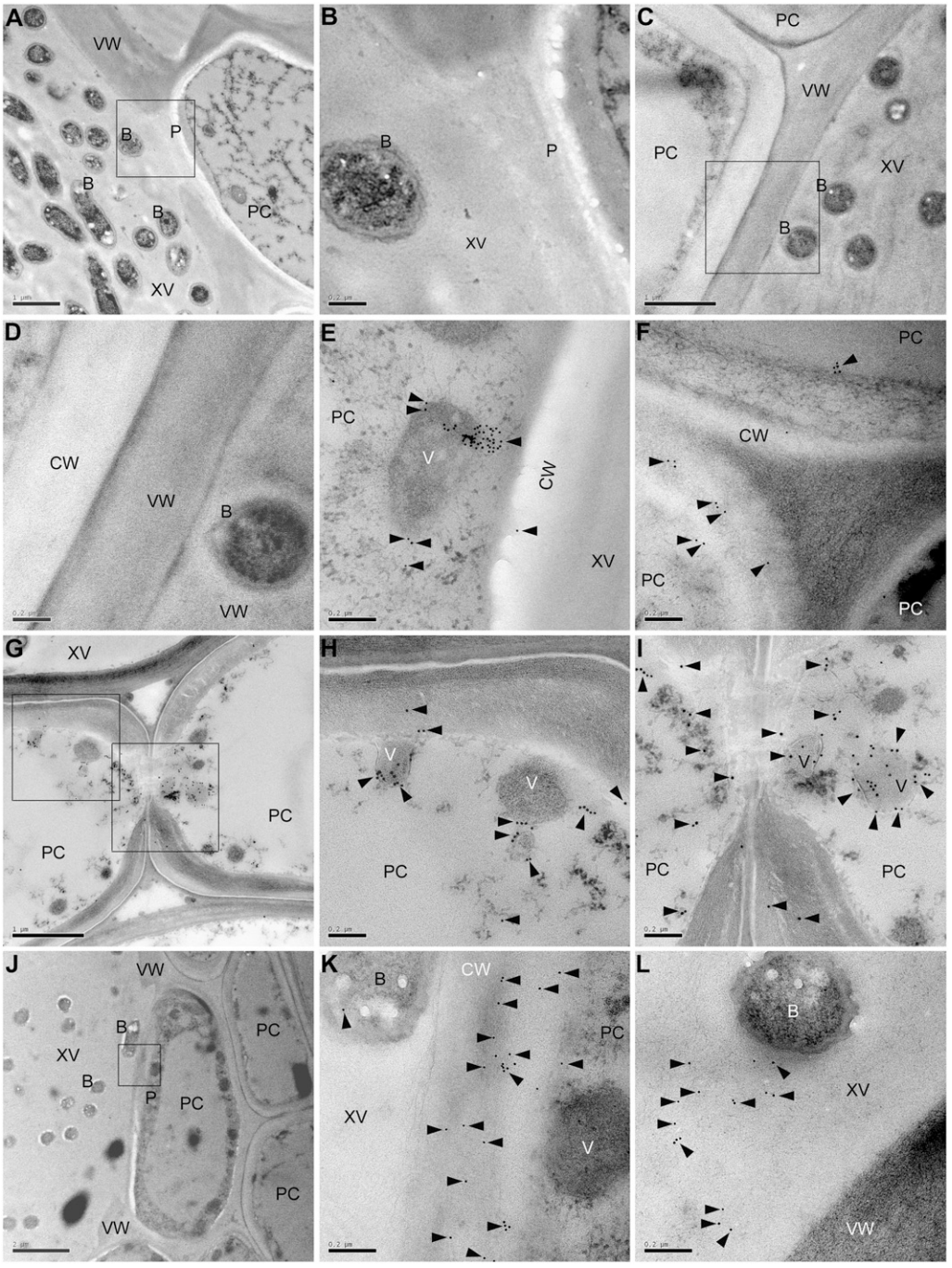

Figure 5. Subcellular localization of XA27-FLAG in leaf vascular elements of L18F of P_{Xa27}:*XA27-FLAG*:T_{Xa27} detected by immunogold electron microscopy. A, Xylem vessel and xylem parenchyma cells of L18F at 3 DAI with *X. oryzae* pv *oryzae* PXO99^{A}. Bar = 1 μm. B, High magnification of the pit area indicated with a box in A. Bar = 0.2 μm. C, Xylem vessel and xylem parenchyma cells of Nipponbare at 3 DAI with PXO99^{A}. Bar = 1 μm. D, High magnification of the cell wall between xylem vessel and xylem parenchyma cells indicated with a box in C. Bar = 0.2 μm. E, Electron-dense vesicles in xylem parenchyma cells near the pit between xylem vessel and xylem parenchyma cells of L18F. Bar = 0.2 μm. F, Cell walls of xylem parenchyma cells of L18F. Bar = 0.2 μm. G, Xylem vessel and xylem parenchyma cells of L18F at 3 DAI with PXO99^{A}. Bar = 1 μm. H, High magnification of the area indicated with a box in G. Bar = 0.2 μm. I, High magnification of the pit area between two xylem parenchyma cells indicated with a box in G. Bar = 0.2 μm. J, Xylem vessel and xylem parenchyma cells of L18F at 3 DAI with PXO99^{A}. Bar = 2 μm. K, High magnification of the pit area between xylem vessel and xylem parenchyma cells indicated with a box in J. Bar = 0.2 μm. L, Xylem vessel and cell wall of xylem parenchyma cells of L18F at 3 DAI with PXO99^{A}. Bar = 0.2 μm. Samples in A and B were probed with preimmune serum. Samples in C to L were detected with anti-FLAG monoclonal antibody. The immune reaction was labeled with 10-nm (A–F, J–L) or 15-nm (G–I) gold-conjugated goat anti-mouse IgG antibody. Gold particles are indicated by arrowheads. B, Bacteria; CW, cell wall; P, pit; PC, xylem parenchyma cell; V, vesicle; VW, vessel wall; XV, xylem vessel.

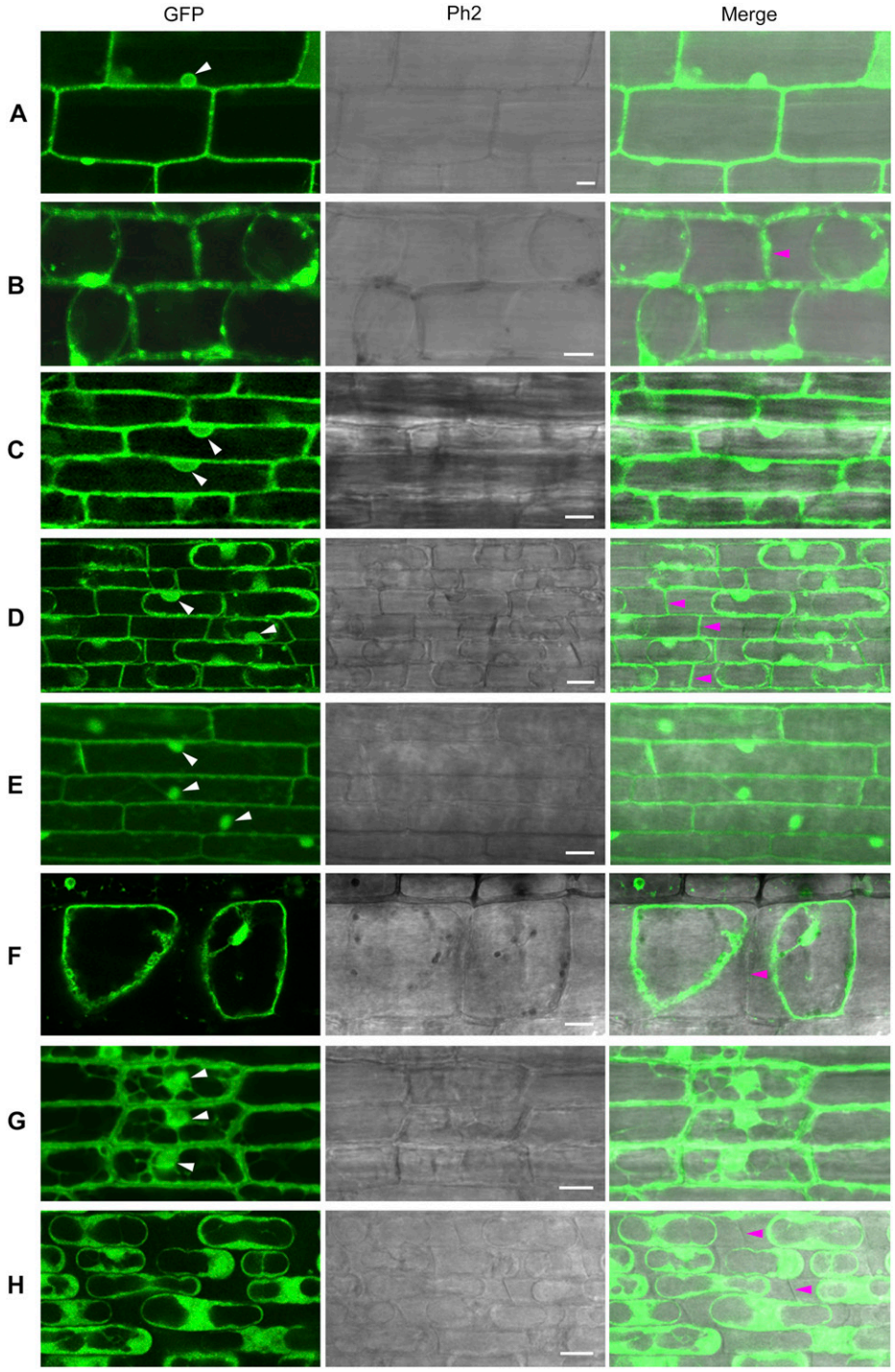

Figure 6. Localization of N57-GFP and N37-GFP in leaf sheath and root cells of transgenic plants. A, Leaf sheath cells of L12 of P_{Ubi}:*N57-GFP*:T_{Nos}. B, Leaf sheath cells of L12 after plasmolysis. C, Root cells of L12. D, Root cells of L12 after plasmolysis. E, Leaf sheath cells of L2 of P_{Ubi}:*N37-GFP*:T_{Nos}. F, Leaf sheath cells of L2 after plasmolysis. G, Root cells of L2. H, Root cells of L2 after plasmolysis. The nuclei are indicated with white arrowheads. Cell walls are indicated with magenta arrowheads. Ph2, Phase Contrast 2. Bars = 10 μm.

Xa27 promoter. We speculate that the *Xa27* promoter is sensitive to its position on the rice chromosome and that the constitutive expression might be due to a position effect on the transgenes in rice chromosomes.

Leaky expression of XA27 or its functional derivatives was found to provide enhanced resistance to compatible pathogen strains. This resistance was dosage dependent. In this study, we selected transgenic lines that retained resistance specificity to incompatible pathogens. The transgenes in these lines were inducible by AvrXa27. We believe that these lines are suitable for determining the localization of XA27 or its fusion proteins, because these fusion proteins confer resistance to the pathogen, indicating their functionality. In addition, the localization of XA27-GFP to the cell walls of leaf sheath and root cells in L22 of P_{Xa27}:

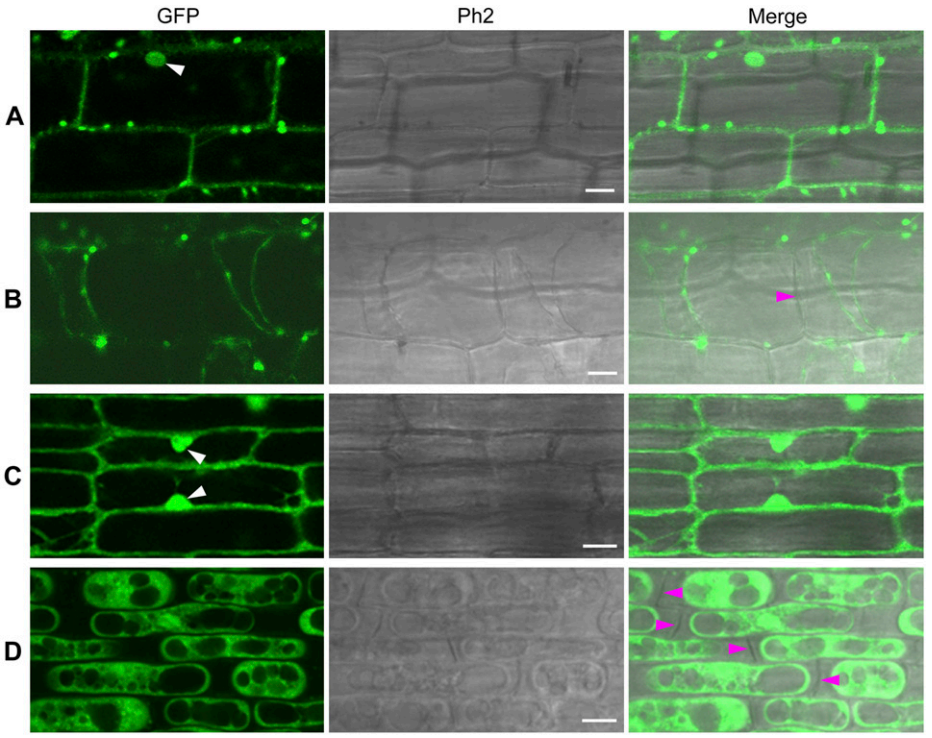

Figure 7. Localization of XA27G-GFP in leaf sheath and root cells of L18G of P_{Ubi}:*XA27G-GFP*:T_{Nos}. A, Leaf sheath cells. B, Leaf sheath cells after plasmolysis. C, Root cells. D, Root cells after plasmolysis. The nuclei are indicated with white arrowheads. Cell walls are indicated with magenta arrowheads. Ph2, Phase Contrast 2. Bars = 10 μm.

XA27-GFP:T_{Xa27} and in L9 of P_{Ubi}:*XA27-GFP*:T_{Nos} gave similar results, which indicates that subcellular localization of XA27-GFP is determined by the nature of the protein. In this case, the localization cannot be explained by any tissue specificity in transgene expression due to the promoter.

The apoplast is the extraprotoplastic matrix of plant cells, consisting of all compartments from the external face of the plasmalemma to the cell wall (Dietz, 1997). The apoplast provides a physical barrier against pathogen attack. It also plays an important role in signaling and defense during plant-pathogen interaction, through the presence of several extracellular enzymes and proteins located in the apoplast or associated with the cell wall (Dietz, 1997; Edreva, 2005; Huckelhoven, 2007). *X. oryzae* pv *oryzae* is a vascular pathogen that enters the rice leaf typically through hydathodes at the leaf tip and leaf margin. It multiplies in the intercellular spaces of the underlying epitheme and thereafter moves to the xylem vessels to cause systemic infection (Noda and Kaku, 1999). The bacteria rely on a type III secretion system to inject virulence effectors into xylem parenchyma cells, probably through the pits between xylem vessels and xylem parenchyma cells. Xylem vessels consist of giant intercellular spaces and form a special apoplast structure. Therefore, the local resistance at xylem parenchyma cells and xylem vessels is important for rice to counterattack the vascular pathogen. For example, the increase in peroxidase activity in extracellular spaces and the accumulation of cationic peroxidase in xylem vessels have been detected during interactions of rice and *X. oryzae* pv *oryzae*, especially during incompatible interactions (Reimers et al., 1992; Young et al., 1995; Hilaire et al., 2001).

Although the biochemical function of XA27 remains to be determined, its localization to xylem vessels may contribute to local resistance to the pathogen at the infection site. XA27 appears to be secreted to the lumina of xylem vessels through the pits between xylem vessels and xylem parenchyma cells. Since xylem parenchyma cells were not suitable for plasmolysis and analysis by confocal microscopy, the localization of XA27-GFP and its derivatives to the apoplast was examined in the leaf sheath cells and in roots of transgenic plants. As the extracellular space or apoplast of leaf sheath cells and root cells is limited, compared with that of xylem vessels, the secreted XA27-GFP protein mainly localizes to the cell wall in these cases. This suggests an extracellular or apoplastic localization of XA27.

Although we lack the means to detect the location of the endogenous XA27 protein, our studies indicate that XA27-FLAG and XA27-GFP proteins localized to the apoplast. XA27 might be secreted to the apoplast by exocytosis, as XA27-FLAG was detected in both cytoplasmic electron-dense vesicles and in the apoplast. The signal-anchor-like sequence of XA27 contains a triple Arg motif, which appears to be essential for both its localization and function. Mutation of this sequence abolished XA27 localization and impaired its ability to confer disease resistance. Similar Arg motifs are also found in the signal peptides of proteins translocated through the twin Arg translocation (Tat)

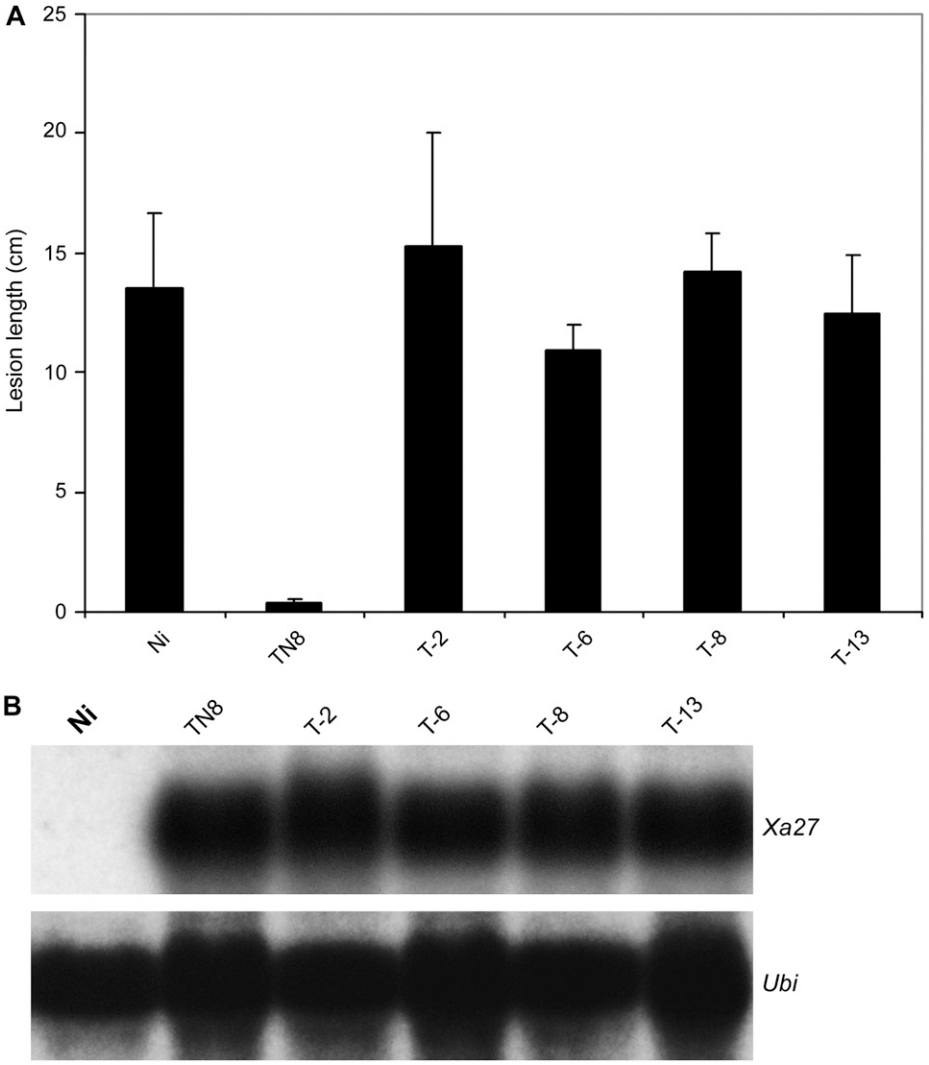

Figure 8. Disease evaluation of transgenic P_{Xa27}:*XA27G*:T_{Xa27} plants to *X. oryzae* pv *oryzae* PXO99^{A} and transgene expression after inoculation. A, Lesion length of bacterial blight on transgenic P_{Xa27}:*XA27G*:T_{Xa27} plants at 14 DAI with PXO99^{A}. Lesion lengths are average values from 16 inoculated leaves with SD. B, Expression of P_{Xa27}:*XA27G*:T_{Xa27} in different transgenic plants (T-2, T-6, T-8, and T-13) at 3 DAI with PXO99^{A}. Ni, Nipponbare; TN8, *Xa27* transgenic line in the Nipponbare background (Gu et al., 2005).

pathway (Robinson and Bolhuis, 2004; Muller and Klosgen, 2005). The Tat pathway is responsible for the export of folded proteins across the cytoplasmic membrane of bacteria or thylakoid membranes of chloroplast in higher plants. Protein transported by the Tat pathway possesses a cleavable signal peptide harboring a twin Arg consensus motif (Robinson and Bolhuis, 2004). The only exception is the Rieske protein from *Paracoccus denitrificans*, which depends on an uncleavable N-terminal Tat signal sequence to anchor it to the cytoplasmic membrane (Bachmann et al., 2006). However, we failed to identify a Tat signal sequence at the N-terminal region of XA27 with the Tat signal prediction server TatP 1.0 (http://www.cbs.dtu.dk/services/TatP/; data not shown).

In conclusion, we have found that the inducible R protein XA27 localizes to the apoplast. This localization depends on a signal-anchor-like sequence at the N-terminal region of XA27 and is required for XA27-mediated resistance to *X. oryzae* pv *oryzae*. The identification of XA27 localization to the apoplast and its localization signal will facilitate further characterization of the biochemical function of the R protein.

MATERIALS AND METHODS

Constructs

The constructs used in this study (Table I) were made based on binary vectors pC1300 or pC1305.1 and verified by DNA sequencing. The *XA27-GFP* fusion gene was generated by PCR with the *Xa27* coding region amplified from NA5.2 (Gu et al., 2005) and the *GFP* coding region amplified from pSSZ41 (Kolesnik et al., 2004). The fused PCR products were cloned into pC1305.1 to generate pCXA27GFP. The *Pst*I fragment of the maize (*Zea mays*) ubiquitin promoter from pSSZ41 was inserted 5′ of the *XA27-GFP* fusion gene in pCXA27GFP to generate pCUXA27GFP. A fragment containing a partial *XA27-GFP* fusion gene was amplified from pCUXA27GFP and cloned into the *Sac*I site of NA5.2 to generate pC27XA27GFP. The *XA27-FLAG* fusion gene was generated by PCR and cloned into the *Spe*I and *Sac*I sites of NA5.2 to generate pC27XA27FLAG. The *N57-GFP* fusion gene was generated by fusing the 5′ coding region of *Xa27*, encoding the first 57 amino acid residues, with the *GFP* gene. The fusion gene was used to replace *XA27-GFP* in pCUXA27GFP to generate pCUN57GFP. Similar methods were used to produce pCUN37GFP, in which the N-terminal 37 amino acid residues of XA27 were fused with GFP. The triple Arg residues in XA27 (residues 27–29) were

replaced with triple Gly residues by PCR. The mutated *Xa27* gene was used to replace wild-type *Xa27* in NA5.2 to generate pC27XA27G. The mutated *Xa27* gene was tagged with *GFP* to give *XA27G-GFP*. This *XA27G-GFP* fusion gene was used to replace *XA27-GFP* in pCUXA27GFP and pC27XA27GFP to produce pCUXA27GGFP and pC27XA27GGFP, respectively. Similar methods were used to generate constructs pCUN57GGFP and pCUN57KGFP, in which the triple Arg residues in the *N57-GFP* fusion gene in pCUN57GFP were replaced with Gly and Lys residues, respectively.

Plant Material and Growth Conditions

Rice (*Oryza sativa*) IRBB27 is a near-isogenic line of *Xa27* in the IR24 background (Gu et al., 2004; Table I). Nipponbare is a *japonica* variety carrying a susceptible *Xa27* allele [*xa27*(Ni); Table I]. TN8 is an *Xa27* transgenic line in the Nipponbare background carrying an *Xa27* genomic subclone of the *Pst*I fragment (Gu et al., 2005; Table I). All rice plants, including those inoculated with *Xanthomonas oryzae* pv *oryzae* strains, were grown in a greenhouse at temperatures ranging from 32°C during the day to 26°C at night, relative humidity averaged 85%, and the photoperiod was 12 to 13 h.

Rice Transformation

Agrobacterium tumefaciens-mediated transformation of Nipponbare rice was carried out as described previously (Yin and Wang, 2000).

Bacterial Blight Inoculation and Disease Scoring

The *X. oryzae* pv *oryzae* strains were cultured on PSA medium (10 g L^{-1} peptone, 10 g L^{-1} Suc, 1 g L^{-1} Glu, and 16 g L^{-1} bacto-agar, pH 7.0) for 2 to 3 d at 28°C. Bacteria were collected and suspended in sterile water at an optical density of 0.5 at 600 nm. Bacterial blight inoculation was carried out using the leaf-clipping method (Kauffman et al., 1973). The disease symptoms were scored according to the criteria described previously (Gu et al., 2004).

Confocal Laser Scanning Microscopy

GFP fluorescence in transgenic plants was examined on the cells of leaves, leaf sheaths, and roots. Leaves of inoculated or uninoculated plants were manually and transversely sectioned with a surgical blade (no. 10). Leaf sheath sections of about 3 × 3 mm^2 and root tips of about 1 cm long were cut from 10-d-old plants. Samples were mounted in water for examination and photography. Plasmolysis was induced on leaf sheath or root cells by incubating the samples in 10% (w/v) mannitol solution for 1 h and mounting in the same solution for examination. Samples were examined for GFP fluorescence with a confocal microscope (Zeiss LSM 510 META) using the excitation/emission combination of 488/505 to 530 nm band pass. The bright-field image was taken simultaneously using Phase Contrast 2 optics.

RNA Gel-Blot Analysis

Total RNA was isolated from rice leaves using the RNeasy Plant Mini Kit (Qiagen) according to the manufacturer's instructions. About 20 μg of total RNA was loaded in each lane for RNA gel-blot analysis. The RNA loading was assessed by staining RNA blots with methylene blue or hybridizing RNA blots with the rice *Ubiquitin2* gene (*Ubi*). DNA probes were labeled with [^{32}P]dCTP using the Rediprime II random prime labeling system (Amersham Biosciences).

Western-Blot Analysis

About 20 μg of total proteins from transgenic plants was separated on 12% SDS polyacrylamide gels followed by blotting onto nitrocellulose membranes. XA27-FLAG proteins were detected with an anti-FLAG-M2 monoclonal antibody (Sigma) and horseradish peroxidase-coupled secondary antibody (Bio-Rad).

Immunogold Electron Microscopy

Immunogold electron microscopy was carried out according to the procedure described previously (Chye et al., 1999). Leaf cross sections of about 3 mm in length were fixed in a solution of 0.5% glutaraldehyde and 2% paraformaldehyde in 0.1 M phosphate buffer for 4 h under vacuum. Specimens were washed with 50 mM phosphate buffer for 45 min. After dehydration in a graded ethanol series, specimens were infiltrated in LR White resin (EMS) and embedded in gelatin capsules. Specimens were sectioned at 80 nm using a Leica Ultracut microtome and mounted on Formvar-coated slotted grids. XA27-FLAG proteins were detected with anti-FLAG monoclonal antibody (Sigma) followed by labeling with 10- or 15-nm gold-conjugated goat anti-mouse IgG antibody (EMS). Mouse preimmune serum was used to substitute anti-FLAG monoclonal antibody in control experiments. Samples on grids were further stained with 2% uranyl acetate and 1% lead citrate. Samples were examined with a transmission electron microscope (JEM-1230; JEOL) operating at 120 kV and photographed with a digital microphotography system (Gatan).

Sequence data from this article can be found in the GenBank/EMBL data libraries under accession number AAY54164.

Supplemental Data

The following materials are available in the online version of this article.

Supplemental Figure S1. Localization of GFP, XA27-GFP, and XA27G-GFP in leaf sheath cells of transgenic plants and 4′,6-diamidino-2-phenylindole staining of nuclei.

Supplemental Figure S2. Localization of XA27-GFP in leaf sheath and root cells of L22 of P_{Xa27}:*XA27-GFP*:T_{Xa27}.

Supplemental Figure S3. Transgene expression in GFP-tagged lines.

Supplemental Figure S4. Localization of N57G-GFP and N57K-GFP in leaf sheath and root cells of transgenic plants.

Supplemental Protocol S1. 4′,6-Diamidino-2-phenylindole staining and GFP fluorescence.

ACKNOWLEDGMENTS

We thank Xuezhi Ouyang, Ao Yin, Qingwen Lin, Dongjiang Wang, and Tze Yee Teo for technical assistance, the Center for the Application of Molecular Biology to International Agriculture for binary vectors pC1300 and pC1305.1, and Stephen Cohen and Mithilesh Mishra for critical reading of the manuscript.

Received May 22, 2008; accepted September 4, 2008; published September 10, 2008.

LITERATURE CITED

Axtell MJ, Staskawicz BJ (2003) Initiation of *RPS2*-specified disease resistance in *Arabidopsis* is coupled to the AvrRpt2-directed elimination of RIN4. Cell **112:** 369–377

Bachmann J, Bauer B, Zwicker K, Ludwig B, Anderka O (2006) The Rieske protein from *Paracoccus denitrificans* is inserted into the cytoplasmic membrane by the twin-arginine translocase. FEBS J **273:** 4817–4830

Boyes DC, Nam J, Dangl JL (1998) The *Arabidopsis thaliana* RPM1 disease resistance gene product is a peripheral plasma membrane protein that is degraded coincident with the hypersensitive response. Proc Natl Acad Sci USA **95:** 15849–15854

Burch-Smith TM, Schiff M, Caplan JL, Tsao J, Czymmek K, Dinesh-Kumar SP (2007) A novel role for the TIR domain in association with pathogen-derived elicitors. PLoS Biol **5:** e68

Chye ML, Huang BQ, Zee SY (1999) Isolation of a gene encoding Arabidopsis membrane-associated acyl-CoA binding protein and immunolocalization of its gene product. Plant J **18:** 205–214

Dangl JL, Jones JDG (2001) Plant pathogens and integrated defense responses to infection. Nature **411:** 826–833

Deslandes L, Olivier J, Peeters N, Feng DX, Khounlotham M, Boucher C, Somssich I, Genin S, Marco Y (2003) Physical interaction between RRS1-R, a protein conferring resistance to bacterial wilt, and PopP2, a

type III effector targeted to the plant nucleus. Proc Natl Acad Sci USA **100:** 8024–8029

Dietz KJ (1997) Function and responses of the leaf apoplast under stress. Prog Bot **58:** 221–254

Edreva A (2005) Pathogenesis-related proteins: research progress in the last 15 years. Gen Appl Plant Physiol **31:** 105–124

Emanuelsson O, Brunak S, von Heijne G, Nielsen H (2007) Locating proteins in the cell using TargetP, SignalP and related tools. Nat Protocols **2:** 953–971

Flor HH (1971) Current status of the gene-for-gene concept. Annu Rev Phytopathol **9:** 275–296

Gu K, Tian D, Yang F, Wu L, Sreekala C, Wang D, Wang GL, Yin Z (2004) High-resolution genetic mapping of Xa27(t), a new bacterial blight resistance gene in rice, Oryza sativa L. Theor Appl Genet **108:** 800–807

Gu K, Yang B, Tian D, Wu L, Wang D, Sreekala C, Yang F, Chu Z, Wang GL, White FF, et al (2005) R gene expression induced by a type-III effector triggers disease resistance in rice. Nature **435:** 1122–1125

Hammond-Kosack KE, Jones JDG (1997) Plant disease resistance genes. Annu Rev Plant Physiol Plant Mol Biol **48:** 575–607

He SY, Nomura K, Whittam TS (2004) Type III protein secretion mechanism in mammalian and plant pathogens. Biochim Biophys Acta **1694:** 181–206

Hilaire E, Young SA, Willard LH, McGee JD, Sweat T, Chittoor JM, Guikema JA, Leach JE (2001) Vascular defense responses in rice: peroxidase accumulation in xylem parenchyma cells and xylem wall thickening. Mol Plant Microbe Interact **14:** 1411–1419

Huckelhoven R (2007) Cell wall-associated mechanisms of disease resistance and susceptibility. Annu Rev Phytopathol **45:** 101–127

Jia Y, McAdams SA, Bryan GT, Hershey HP, Valent B (2000) Direct interaction of resistance gene and avirulence gene products confers rice blast resistance. EMBO J **19:** 4004–4014

Kauffman HE, Reddy APK, Hsieh SPY, Merca SD (1973) An improved technique for evaluating resistance to rice varieties of *Xanthomonas oryzae*. Plant Dis Rep **57:** 537–541

Kim YJ, Lin NC, Martin GB (2002) Two distinct *Pseudomonas* effector proteins interact with the Pto kinase and activate plant immunity. Cell **109:** 589–598

Kolesnik T, Szeverenyi I, Bachmann D, Kumar CS, Jiang S, Ramamoorthy R, Cai M, Ma ZG, Sundaresan V, Ramachandran S (2004) Establishing an efficient *Ac/Ds* tagging system in rice: large-scale analysis of *Ds* flanking sequences. Plant J **37:** 301–314

Lauge R, De Wit PJ (1998) Fungal avirulence genes: structure and possible functions. Fungal Genet Biol **24:** 285–297

Lee SW, Han SW, Bartley LE, Ronald PC (2006) Unique characteristics of *Xanthomonas oryzae* pv. *oryzae* AvrXa21 and implications for plant innate immunity. Proc Natl Acad Sci USA **103:** 18395–18400

Leister RT, Katagiri F (2000) A resistance gene product of the nucleotide binding site-leucine rich repeats class can form a complex with bacterial avirulence proteins in vivo. Plant J **22:** 345–354

Martin GB, Bogdanove AJ, Sessa G (2003) Understanding the functions of plant disease resistance proteins. Annu Rev Plant Biol **54:** 23–61

Mew TW (1987) Current status and future prospects of research on bacterial blight of rice. Annu Rev Phytopathol **25:** 359–382

Muller M, Klosgen RB (2005) The Tat pathway in bacteria and chloroplasts: review. Mol Membr Biol **22:** 113–121

Nimchuk Z, Marois E, Kjemtrup S, Leister RT, Katagiri F, Dangl JL (2000) Eukaryotic fatty acylation drives plasma membrane targeting and enhances function of several type III effector proteins from *Pseudomonas syringae*. Cell **101:** 353–363

Noda T, Kaku H (1999) Growth of *Xanthomonas oryzae* pv. *oryzae* in planta and in guttation fluid of rice. Ann Phytopathological Soc Jpn **65:** 9–14

Reimers PJ, Guo A, Leach JE (1992) Increased activity of a cationic peroxidase associated with an incompatible interaction between *Xanthomonas oryzae* pv. *oryzae* and rice (*Oryza sativa*). Plant Physiol **99:** 1044–1050

Rivas S, Thomas CM (2005) Molecular interactions between tomato and the leaf mold pathogen *Cladosporium fulvum*. Annu Rev Phytopathol **43:** 395–436

Robinson C, Bolhuis A (2004) Tat-dependent protein targeting in prokaryotes and chloroplasts. Biochim Biophys Acta **1694:** 135–147

Scofield SR, Tobias CM, Rathjen JP, Chang JH, Lavelle DT, Michelmore RW, Staskawics BJ (1996) Molecular basis of gene-for-gene specificity in bacterial speck disease of tomato. Science **274:** 2063–2065

Shen QH, Saijo Y, Mauch S, Biskup C, Bieri S, Keller B, Seki H, Ulker B, Somssich IE, Schulze-Lefert P (2007) Nuclear activity of MLA immune receptors links isolate-specific and basal disease-resistance responses. Science **315:** 1098–1103

Song WY, Wang GL, Chen LL, Kim HS, Pi LY, Holsten T, Gardner J, Wang B, Zhai WX, Zhu LH, et al (1995) A receptor kinase-like protein encoded by the rice disease resistance gene, Xa21. Science **270:** 1804–1806

Tang X, Frederick RD, Zhou J, Halterman DA, Jia Y, Martin GB (1996) Initiation of plant disease resistance by physical interaction of AvrPto and Pto kinase. Science **274:** 2060–2063

von Heijne G (1988) Transcending the impenetrable: how proteins come to terms with membranes. Biochim Biophys Acta **947:** 307–333

Yin Z, Wang GL (2000) Evidence of multiple complex patterns of T-DNA integration into the rice genome. Theor Appl Genet **100:** 461–470

Young SA, Guo A, Guikema JA, White FF, Leach JE (1995) Rice cationic peroxidase accumulates in xylem vessels during incompatible interactions with *Xanthomonas oryzae* pv. *oryzae*. Plant Physiol **107:** 1333–1341